Validation of satellite formaldehyde (HCHO) retrievals using observations from 12 aircraft campaigns

Lei Zhu[1,2], Gonzalo González Abad[1], Caroline R. Nowlan[1], Christopher Chan Miller[1], Kelly Chance[1], Eric C. Apel[3], Joshua P. DiGangi[4], Alan Fried[5], Thomas F. Hanisco[6], Rebecca S. Hornbrook[3], Lu Hu[7], Jennifer Kaiser[8,9], Frank N. Keutsch[10,11,12], Wade Permar[7], Jason M. St. Clair[6,13], Glenn M. Wolfe[6,13]

[1]Harvard-Smithsonian Center for Astrophysics, Cambridge, MA, USA
[2]School of Environmental Science and Engineering, Southern University of Science and Technology, Shenzhen, China
[3]Atmospheric Chemistry Observations & Modeling Laboratory, National Center for Atmospheric Research, Boulder, CO, USA
[4]NASA Langley Research Center, Hampton, VA, USA
[5]Institute of Arctic & Alpine Research, University of Colorado, Boulder, CO, USA
[6]Atmospheric Chemistry and Dynamic Laboratory, NASA Goddard Space Flight Center, Greenbelt, MD, USA
[7]Department of Chemistry and Biochemistry, University of Montana, Missoula, MT, USA
[8]School of Civil and Environmental Engineering or Earth, Georgia Institute of Technology, Atlanta, GA, USA
[9]School of Earth and Atmospheric Sciences, Georgia Institute of Technology, Atlanta, GA, USA
[10]John A. Paulson School of Engineering and Applied Sciences, Harvard University, Cambridge, MA 02138, USA
[11]Department of Chemistry and Chemical Biology, Harvard University, Cambridge, MA 02138, USA
[12]Department of Earth and Planetary Sciences, Harvard University, Cambridge, MA 02138, USA
[13]Joint Center for Earth Systems Technology, University of Maryland Baltimore County, Baltimore, MD, 21228, USA

Correspondence to: Lei Zhu (zhul3@sustech.edu.cn)

Abstract. Formaldehyde (HCHO) has been measured from space for more than two decades. Owing to its short atmospheric lifetime, satellite HCHO data are used widely as a proxy of volatile organic compounds (VOCs; please refer to Appendix A for abbreviations and acronyms), providing constraints on underlying emissions and chemistry. However, satellite HCHO products from different satellite sensors using different algorithms have received little validation so far. The accuracy and consistency of HCHO retrievals remain largely unclear. Here we develop a validation platform for satellite HCHO retrievals using *in situ* observations from 12 aircraft campaigns with a chemical transport model (GEOS-Chem) as the intercomparison method. Application to the NASA operational OMI HCHO product indicates negative biases (–44.5% to –21.7%) under high-HCHO condition while high biases (+66.1% to +112.1%) under low-HCHO conditions. Under both conditions, HCHO *a priori* vertical profiles are likely not the main driver of the biases. By providing quick assessment to systematic biases in satellite products over large domains, the platform facilitates, in an iterative process, optimization of retrieval settings and the minimization of retrieval biases. It is also complementary to localized validation efforts based on ground observations and aircraft spirals.

1 Introduction

Formaldehyde (HCHO) is ubiquitous in the troposphere due to its high product yields from atmospheric oxidation of volatile
organic compounds (VOCs). Methane mainly controls the tropospheric background, whereas regional enhancements are contributed largely by short-lived non-methane VOCs (NMVOCs) emitted from the biosphere, human activities, and wildfires. HCHO is detectable from space using solar ultraviolet backscattered radiation between 325 and 360 nm [Chance et al., 2000]. HCHO vertical column densities (VCDs; in the unit of molecules cm^{-2}) are obtained after the retrieval process and the consideration of *a priori* information. Because of the short atmospheric lifetime of HCHO (a few hours), satellite HCHO VCD has been used as a localized proxy for NMVOC emissions [*e.g.*, Palmer et al., 2003; Shim et al., 2005; Stavrakou et al., 2009; Marais et al., 2012; Barkley et al., 2013; Zhu et al., 2014; Zhu et al., 2017a; Cao et al., 2018; Surl et al., 2018]. In addition, previous applications of HCHO retrievals also include evaluating surface ozone sensitivity [Jin and Holloway, 2015; Jin et al., 2017], quantifying cancer risks of ambient HCHO [Zhu et al., 2017b], estimating organic aerosol abundance [Liao et al., 2019], and mapping hydroxyl (OH) radicals [Wolfe et al., 2019]. However, validation of satellite HCHO products from different satellite sensors using different algorithms have received little attention so far. Validation exercises over different regions in different seasons remain extremely limited. Here we develop a validation platform built with HCHO observations from 12 aircraft campaigns over the United States, Eastern Asia, and the remote Pacific Ocean. We further apply it to the NASA operational HCHO product and report the validation results.

HCHO has been continuously observed from space for more than two decades since GOME (1996–2003) [Chance et al., 2000; De Smedt et al., 2008] and SCIAMACHY (2003–2012) [Wittrock et al., 2006; De Smedt et al., 2008]. Presently available observations are from OMI (2004–) [De Smedt et al., 2015; González Abad et al., 2015], GOME-2A (2006–) [De Smedt et al., 2012], OMPS (2011–) [Li et al., 2015; González Abad et al., 2016], GOME-2B (2012–) [De Smedt et al., 2012], and TROPOMI (2018–) [De Smedt et al., 2018]. Hourly HCHO observations (in daytime) will be made available from a constellation of geostationary satellites to be launched in the coming 1–3 years, including GEMS (2020) [Kim et al., 2019; Kwon et al., 2019] over Eastern Asia, TEMPO (2022) [Zoogman et al., 2017] over North America, and Sentinel-4 (2023) [Courrèges-Lacoste et al., 2017] over Europe. HCHO retrieved from the above satellites generally follows a two-step approach, slant column density (SCD) fitting and conversion of it to VCD using localized air mass factors (AMFs), with retrieval errors being introduced in each step [Marais et al., 2012; De Smedt et al., 2015; González Abad et al., 2015; Hewson et al., 2015; Kwon et al., 2017; Herman et al., 2018; Nowlan et al., 2018].

Previous validation of HCHO satellite data sets is often conducted by directly comparing coincident satellite pixels and observation points. Wittrock et al. [2006] and Vigouroux et al. [2009] found SCIAMACHY HCHO columns are unbiased compared with ground-based measurements over remote regions. De Smedt et al. [2015] reported OMI and GOME2 data are –20% to –40% biased against observed vertical profiles. Wang et al. [2017] reported biases in OMI and GOME2 data

of –12% to –20% over the Eastern China from May to December. A recent study showed monthly bias in OMI data ranges from –11% in summer to +26% in winter in Beijing between 2010 and 2016 [Wang et al., 2019]. Comparison with aircraft observations indicated that GOME data are +16% biased during summer over Eastern Texas in the United States [Martin et al., 2004], and that OMI data are biased by –37% in October over Guyana [Barkley et al., 2013]. Tan et al. [2018] found OMPS data are –18% biased against ship-based measurements in June over the East China Sea.

Such direct validation approaches, however, face three practical challenges. First, they require the averaging of extensive observations to reduce large random noises associated with individual satellite retrievals. Second, they fail to make full use of precise *in situ* observations. Low earth orbit (LEO) satellites pass over a certain location within a fixed time window up to a couple of times per day, meaning only a small fraction of observations are coincident with satellite pixels thus suitable for the purpose of direct validation. Finally, reliability of validation results is unclear for areas beyond the observation sites/domains.

Alternatively, Zhu et al. [2016] proposed an indirect validation approach with a chemical transport model (CTM) as the intercomparison method. This approach increases considerably the range of data and conditions that can be used for validation, and therefore reduces random noises in satellite retrievals through averaging. Using this approach, Zhu et al. [2016] found current HCHO satellite products are biased by –20% to –51% against the SEAC^{4}RS [Toon et al., 2016] aircraft measurements over the Southeastern United States during the summer of 2013. Here we follow this indirect validation approach to develop a validation platform for satellite HCHO retrievals using observations from 12 aircraft campaigns all over the world, as discussed below.

2 HCHO observations from aircraft campaigns

Figure 1 shows flight tracks of 12 aircraft campaigns used in this study. Detailed information is summarized in Table 1. The 12 aircraft campaigns are selected based on the data availability and spatial representativeness. Together, the 12 aircraft campaigns offer exceptional opportunities for validating of satellite HCHO retrievals with extensive observations over the United States (C1–C9; DISCOVER-AQ California 2013, NOMADSS, SENEX, DISCOVER-AQ Texas 2013, DISCOVER-AQ Colorado 2014, FRAPPÉ, WINTER, SONGNEX, and WE-CAN, respectively), Eastern Asia (C10; KORUS-AQ), and the remote Pacific Ocean (C11–C12; ATom-1 and ATom-2). The aircraft campaigns have great spatial coverages over HCHO hotspots, such as the Southeastern United States (C2 and C3) dominated by strong biogenic isoprene emissions [Guenther et al., 2012], Houston area (C4) featured with high anthropogenic NMVOCs [Zhu et al., 2014], and the Western United States (C9) influenced by wildfires. The campaigns also survey different seasons of the year, enabling assessment of seasonal biases in satellite HCHO products.

3

During the aircraft campaigns, HCHO observations were made along the flight tracks with multiple instruments, including (1) NCAR Difference Frequency Generation Absorption Spectrometer (DFGAS) [Weibring et al., 2006, 2007, 2010], (2) Trace Organic Gas Analyzer (TOGA) [Apel et al., 2003; 2010; 2015], (3) In Situ Airborne Formaldehyde instrument (ISAF) [Cazorla et al., 2015], (4) Compact Atmospheric Multispecies Spectrometer (CAMS) [Fried et al., 2011; Richter et al., 2015], and (5) Proton Transfer Reaction Time-of-Flight Mass Spectrometer (PTR-ToF-MS) [Müller et al., 2014]. The instrument accuracy (1σ level) is 4.5%, 15% (lower limit; https://airbornescience.nasa.gov/instrument/TOGA), 10% [Cazorla et al., 2015], 4% [Richter et al., 2015], and 60% [Hu and Permar, 2019] for DFGAS, TOGA, ISAF, CAMS, and PTR-ToF-MS, respectively. The corresponding instrument detection limits are 40–100 ppt [Nowlan et al., 2018], 20 ppt [Wofsy et al., 2018], 36 ppt [Cazorla et al., 2015], ~ 40 ppt [Richter et al., 2015] and 300 ppt [Hu and Permar, 2019], respectively.

HCHO observations from different instruments are generally consistent. Zhu et al. [2016] reported ISAF to be in good agreement with CAMS during the SEAC^{4}RS campaign with a correlation coefficient (r) of 0.99 and a slope of 1.10. ISAF is also found consistent (r=0.98) with DFGAS during the DC3 campaign [Barth et al., 2015] with a slope of 1.07 [Liao et al., 2019]. Figure 2 shows point-to-point comparisons among 1-min averaged TOGA, ISAF, and CAMS HCHO observations aboard the aircrafts. There is a high correlation in the mixed layer (here and elsewhere defined as below 2 km; r=0.86) and free troposphere (> 2 km; r=0.93) between TOGA and CAMS during the FRAPPÉ campaign with a Reduced major axis (RMA) regression slope of 1.05±0.01. During the WINTER campaign, TOGA generally matches with ISAF (r=0.72) within the mixed layer. However, consistency between the two instruments begins to fall apart in the free troposphere (r=0.33), which is likely driven by sampling differences. TOGA correlates highly with ISAF during the ATom-2 (C12) campaign in both mixed layer (r=0.83) and free troposphere (r=0.82), but overall it is 48% higher than ISAF likely due to the fact that the two instruments are independently calibrated. In this study, we use CAMS data for FRAPPÉ (C6), ISAF data for both WINTER (C7) and ATom-2 (C12), given their higher accuracies.

Figure 3 shows mean vertical profiles measured from the 12 aircraft campaigns. For campaigns conducted over/near land (C1–C10), aircraft observations show higher level of HCHO within the mixed layer as a result of biogenic and anthropogenic NMVOC emissions. In the free troposphere, HCHO starts to drop sharply due to short lifetimes of highly reactive NMVOCs, such as isoprene (~ 1 h) and HCHO itself (~ 2 h). We see enhanced HCHO (> 3 ppb) in 3–5 km during the WE-CAN (C9) campaign, which is caused by intensive primary and secondary production of HCHO from wildfires in the Western United States. Mean HCHO over the remote Pacific Ocean (C11–C12) declines with altitudes through the troposphere (below 12 km), suggesting oxidation of well-mixed methane as the dominant source of the tropospheric background HCHO.

3 GEOS-Chem as the intercomparison method

130   The indirect validation approach requires a CTM to bridge sampling gaps between aircraft observations and satellite retrievals [Zhu et al., 2016]. Here we use GEOS-Chem version 12.0.0 (doi:10.5281/zenodo.1343547) as the intercomparison method for validation of satellite HCHO columns using aircraft observations. With a detailed representation of ozone-NO_x-VOCs-aerosol-halogens tropospheric chemistry, the GEOS-Chem model has been used extensively in several studies to simulate HCHO including comparisons with *in situ* observations [Jaeglé et al., 2015; Zhu et al., 2016; Chan Miller et al., 135 2017; Liao et al., 2019]. Zhu et al. [2016] and Chan Miller et al. [2017] found that GEOS-Chem provides an unbiased simulation of SEAC^{4}RS and SENEX aircraft observations within the mixed layer over the Southeastern United States in summer, including horizontal patterns and mean vertical profiles. In winter, GEOS-Chem is biased by −32% compared against aircraft observations below 300 m over the Northeastern United States [Jaeglé et al., 2015].

140   The GEOS-Chem model is driven by the Goddard Earth Observing System–Forward Processing (GEOS-FP) assimilated meteorological data, produced by the NASA Global Modeling and Assimilation Office (GMAO) [Molod et al., 2012]. The GEOS-FP meteorological data have a native horizontal resolution of 0.25°×0.3125° with 72 vertical pressure levels and 3 h temporal frequency (1 h for surface variables and mixed layer depths). Biogenic VOC emissions are from the MEGAN 2.1 model [Guenther et al., 2012] as implemented in GEOS-Chem by Hu et al. [2015]. Anthropogenic emissions are based on 145 the NEI2011 inventory [EPA, 2015] over the United States, and the MIX inventory [Li et al., 2017] over the Eastern Asia region. Fire emissions are from the fourth-generation global fire emissions database (GFED4) [Giglio et al., 2013]. Surface-driven vertical mixing up to the mixing depth is based on the non-local mixing scheme of Holtslag and Boville [1993], as implemented in GEOS-Chem by Lin and McElroy [2010].

150   We run the GEOS-Chem model at a 2°×2.5° resolution to simulate the ATom-1 (C11) and ATom-2 (C12) campaigns as HCHO over the remote Pacific Ocean is relatively homogeneously distributed due to methane oxidation. Over the continents, we use the native resolution (0.25°×0.3125°, nested version) in GEOS-Chem to better represent heterogeneities in emissions and chemistry during the aircraft campaigns (C1–C10) over North America (130°–60°W, 9.75°–60°N) and Eastern Asia (70°–140°E, 15°–55°N). Dynamic boundary conditions for the nested simulations are from global 2°×2.5° runs. Global and 155 nested simulations are spun up for 10 and 1 month, respectively, to remove the sensitivity to initial conditions. GEOS-Chem is sampled along the flight tracks at the time and locations of the aircraft measurements.

    Figure 3 shows GEOS-Chem mean HCHO profiles. Previous studies [Scarino et al., 2014; Millet et al., 2015; Zhu et al., 2016] found GEOS-FP mixing depth in summer is biased low comparing with observations by a factor of 30%–50%, which 160 may partially contribute to the underestimation of HCHO in the mixed layer (Figure 3) by GEOS-Chem over the Unites States (C1–C6, C9) and South Korea (C10). On top of that, underestimation of highly reactive VOC emissions as reported by

Zhu et al. [2014] may be another reason for the lower simulated HCHO over Houston area (C4). GEOS-Chem generally reproduces the observed vertical distribution of HCHO in the free troposphere. Exceptions are for campaigns surveying the Western United States in summer (C5, C6, and C9), likely caused by uncertainties in GFED4 fire emissions in the model.

165

By integrating the mean vertical profiles in Figure 3, we estimate, for each aircraft campaign, a mean observed HCHO column, a mean GEOS-Chem modeled HCHO column, and the regional bias associated with GEOS-Chem model as informed by comparison between observed and modelled HCHO columns. Figure 3 shows the regional bias for each aircraft campaign, which is later applied as the correction factor in the validation exercises.

170 **4 Application to NASA operational HCHO product**

NASA operational OMI HCHO product is based on the Smithsonian Astrophysical Observatory (SAO) HCHO retrieval algorithm [González Abad et al., 2015]. Briefly, the algorithm follows a two-step approach. First, a reference sector correction term (Ω_{S0}) is subtracted from the fitted total SCD (Ω_S), yielding the reference sector corrected SCD ($\Delta\Omega_S$):

$$\Delta\Omega_S = \Omega_S - \Omega_{S0} \tag{1}$$

175 Following Khokhar et al. (2005) and De Smedt et al. (2008), the reference sector correction (Ω_{S0}) represents a daily post-processing normalization for the retrieved SCD, calculated as the difference between the retrieved SCD over the Pacific Ocean and the GEOS-Chem VCD climatology over the Pacific Ocean multiplied by satellite air mass factor (*AMF*) (González Abad et al., 2015; González Abad et al., 2016). $\Delta\Omega_S$ is then converted to VCD (Ω) by applying corresponding *AMF*:

180 $$\Omega = \frac{\Delta\Omega_S}{AMF} \tag{2}$$

The *AMF* depends on a number of factors, including solar zenith angle (θ_Z), satellite viewing angle (θ_V), cloud characteristics, scattering properties of the atmosphere and surface, and HCHO *a priori* profiles. Following Palmer et al. [2001], it is computed as the product of a geometrical *AMF* (AMF_G) and a correction with scattering weights w applied to the vertical shape factors S:

185 $$AMF = AMF_G \int_{P_S}^{0} w(p)S(p)dp \tag{3}$$

$$AMF_G = \sec\theta_Z + \sec\theta_V \tag{4}$$

Here the integration is over the pressure (p) coordinate from the surface (P_S) to the top of atmosphere. S is the normalized vertical profile of HCHO mixing ratios $C(p)$:

$$S(p) = \frac{C(p)\Omega_A(p)}{\int_{P_S}^{0} C(p)\Omega_A(p)dp} \tag{5}$$

190 where $\Omega_A(p)$ is the partial air column density at p, and w measure the sensitivity of the backscattered radiation to HCHO. OMI SAO HCHO product provides Ω, Ω_S, $\Delta\Omega_S$, AMF_G (in term of θ_Z and θ_V), *AMF*, S, and w for each pixel. Uncertainties

associated with Ω are 30%–100%, contributed by uncertainties in both *AMF* (~ 35%) and $\Delta\Omega_S$ (30–100%) [González Abad et al. 2015].

195   Here we use the DISCOVER-AQ 2013 (C1) flight campaign as an example to demonstrate the validation process. Validation of OMI SAO HCHO product starts with the selection of satellite pixels. This is done for each campaign within the corresponding study period (Table 1) and domain (defined in Table 1; shown in Figure 1) based on following criteria: (1) pass quality checks (MainDataQualityFlag=0), (2) have cloud fraction less than 0.3, (3) have θ_Z less than 60°, and (4) have VCD within the range of -8.0×10^{15} molecules cm^{-2} to 7.6×10^{16} molecules cm^{-2}. The last criterion is set based on 3 times of
200 the fitting uncertainty (30%–100%) and a typical VCD value between 4.0×10^{15} molecules cm^{-2} and 4×10^{16} molecules cm^{-2} [González Abad et al. 2015]. We then compute campaign-averaged GEOS-Chem HCHO columns by sampling the model according to OMI's schedule. The original GEOS-Chem columns are further scaled using correction factors informed by comparison of model and aircraft columns (Figure 3). Figure 4 shows campaign-averaged HCHO columns for both OMI SAO and corrected GEOS-Chem over the study domain (California, United States). Campaign-averaged OMI and corrected
205 GEOS-Chem HCHO columns for other campaigns (C2–C12) are in the Supplement. Poor spatial correlations between OMI and corrected GEOS-Chem columns during some campaigns (Figure 4 and Supplement) likely reflect large uncertainties in OMI columns. Finally, we compare spatially and temporally averaged HCHO columns, during the study period and over the study domain, as reported by OMI SAO product and modelled by GEOS-Chem (with correction) to estimate the regional systematic bias in OMI SAO HCHO product. Detailed validation results are summarized in Table 2.

210

    We see from Table 2 that relative biases in OMI HCHO product depends on both locations and seasons, ranging from –44.5% in summer (C9) to +112.1% in spring (C8) both over the Western United States. Overall, the relative biases in OMI SAO product fall into two categories. First, the product is negatively biased (–44.5% to –21.7%) under high-HCHO conditions (arbitrarily defined as mean HCHO column > 1.0×10^{16} molecules cm^{-2}), such as summertime Southeastern (C2,
215 C3, C4) and Western (C9) United States as well as summertime South Korea (C10). A similar bias (–37.0%) in OMI SAO HCHO product is reported by Zhu et al. [2016] for summertime Southeastern United States. Second, the product is highly biased (+66.1% to +112.1%) under low-HCHO conditions, such as the Western United States (C5, C6, and C8), wintertime United States (C1 and C7), and the remote Pacific Ocean (C11 and C12). Our work points to a higher bias (~ 70%) in OMI SAO retrievals over the remote Pacific Ocean compared with the bias (~ 10%) reported by Wolfe et al. [2019]. This is likely
220 driven by a number of factors: (1) Wolfe et al. [2019] use all data, whereas we only use data over the Pacific region (Figure 1); (2) selection criteria (e.g., θ_Z and data filtering) for OMI pixels are different; (3) mean observed HCHO column is computed from individual profiles in Wolfe et al. [2019], while it is computed based on a mean profile in this study; (4) and finally, the relative bias metric is more sensitive to absolute bias under low-HCHO conditions.

225 In both cases, *a priori* vertical profiles used in the SAO HCHO retrieval algorithm are likely not the main drivers of the biases. SAO HCHO algorithm samples HCHO shape factors (S) from a monthly mean climatology based on GEOS-Chem simulations in 2007 at a spatial resolution of $2°\times2.5°$, which may not be able to represent the spatial heterogeneity in chemistry, nor/or to model temporal variations in emissions. In the first case, after recomputing the AMF with observed HCHO shape factors following equation (3)–(5), relative biases in HCHO reduce slightly on average from –36.5% to –

230 32.6% (C3, C4, C9, and C10 in Table 2). The largest improvement is seen for C3 and C4, where relative biases are reduced on average from –35.4% to –27.4%, because using observed HCHO shape factors results in lower AMF by correcting underestimated *a priori* HCHO within the mixed layer (Figure 5). During the WE-CAN campaign (C9), recomputed AMF is slightly higher than that reported by OMI (Table 2) because of elevated HCHO around 3–5 km from wildfire plumes (Figure 5). In the second case, using observed HCHO shape factors, however, barely reduces biases in OMI SAO HCHO product

235 (Table 2).

Reference sector corrected SCD ($\Delta\Omega_S = \Omega_S–\Omega_{S0}$) and/or other AMF components (such as surface reflectivity and cloud correction) are likely the main drivers of high biases. This can be further examined with aircraft observations and OMI HCHO pixels over remote Pacific Ocean (C11 and C12), where contribution of Ω_{S0} to $\Delta\Omega_S$ is much lower (~ 18%; Table 2).

240 Integration of ATom1 (C11) and ATom2 (C12) vertical profiles indicates a Pacific background HCHO VCD of ~ 3.0×10^{15} molecules cm^{-2} (Figure 3), comparable with previous measured values (2.8×10^{15} molecules cm^{-2} to 4.6×10^{15} molecules cm^{-2}) over the remote North Pacific Ocean [Singh et al., 2009] and modeled results (4.5×10^{15} molecules cm^{-2}) [Wolfe et al., 2019]. This is equivalent to a background SCD of ~ 4.7×10^{15} molecules cm^{-2} with AMF computed using observed HCHO shape factors (Figure 5). OMI SAO SCD (Ω_S) and reference sector corrected SCD ($\Delta\Omega_S$) is much higher than such estimated

245 background SCD value by a factor of ~ 2.0 (Table 2), pointing to potential issues with SCD fitting and/or reference sector correction in the SAO HCHO retrieval algorithm.

We attribute the remaining biases to increased impact of interferers (*e.g.*, O_3 and BrO, O_2-O_2 and water vapor) when HCHO signals are weak. We also find that OMI SAO HCHO VCD correlates moderately (r=0.38 to 0.66) with surface albedo

250 during some campaigns (*i.e.*, C1, C5, and C6), suggesting possible bias introduced by using a reflectance climatology [Kleipool et al., 2008] in the retrievals. In summary, high biases under low-HCHO conditions are likely driven by both reference sector correction and SCD fitting. An updated SAO product is being developed to minimize the biases by optimizing the two processes accordingly.

5 Conclusions

255 We have used HCHO observations from 12 aircraft campaigns, together with the GEOS-Chem chemical transport model as an intercomparison method, to develop a validation platform for satellite HCHO retrievals. The validation platform offers an

8

alternative way to quickly assess systematic biases in satellite products over large spatial domains and longer temporal periods, facilitating optimization of retrieval settings and the minimization of retrieval biases. Application to NASA operational HCHO product (SAO retrievals) indicates that relative biases range from –44.5% to +112.1% depending on locations and seasons. The product is negatively biased (–44.5% to –21.7%) under high-HCHO conditions, such as summertime Southeastern United States,, while positively biased (+66.1% to +112.1%) under low-HCHO conditions, such as wintertime United States and remote Pacific Ocean. Under both conditions, HCHO *a priori* vertical profiles are likely not the main driver of the biases. Our work points to the need for improvement in OMI SAO HCHO product to correct the systematic biases, particularly, optimization of the HCHO slant column fitting and reference sector correction.

Data and code availability

The validation platform (R scripts) is available at: https://doi.org/10.7910/DVN/KG3XNC.

The GEOS-Chem model is available at http://acmg.seas.harvard.edu/geos/ (last access: Nov. 29, 2019).

OMI-SAO HCHO data were downloaded from http://disc.sci.gsfc.nasa.gov/Aura/dataholdings/OMI/omhcho_v003.shtml.

Aircraft observations are available respectively as following:

DISCOVER-AQ California 2013 (C1): https://www-air.larc.nasa.gov/missions/discover-aq/discover-aq.html

NOMADSS (C2): https://www.eol.ucar.edu/field_projects/nomadss/

SENEX (C3): https://www.esrl.noaa.gov/csd/projects/senex/

DISCOVER-AQ Texas 2013 (C4): https://www-air.larc.nasa.gov/missions/discover-aq/discover-aq.html

DISCOVER-AQ Colorado 2014 (C5): https://www-air.larc.nasa.gov/missions/discover-aq/discover-aq.html

FRAPPÉ (C6): http://catalog.eol.ucar.edu/FRAPPE/

WINTER (C7): http://catalog.eol.ucar.edu/winter/

SONGNEX (C8): https://www.esrl.noaa.gov/csd/projects/songnex/

WE-CAN (C9): https://www.eol.ucar.edu/field_projects/we-can/

KORUS-AQ (C10): https://www-air.larc.nasa.gov/missions/korus-aq/

ATom-1 (C11): https://daac.ornl.gov/ATOM/campaign/

ATom-2 (C12): https://daac.ornl.gov/ATOM/campaign/

Appendix A

Abbreviations and acronyms

AMF	Air mass factor
AMF_G	Geometrical Air mass factor
ATom	Atmospheric Tomography Mission

	CAMS	Compact Atmospheric Multispecies Spectrometer
	CTM	Chemical transport model
	DC3	Deep Convective Clouds and Chemistry Experiment
290	DFGAS	Difference Frequency Generation Absorption Spectrometer
	DISCOVER-AQ	Deriving Information on Surface Conditions from COlumn and VERtically Resolved Observations Relevant to Air Quality
	FRAPPÉ	Front Range Air Pollution and Photochemistry Éxperiment
	GEMS	Geostationary Environment Monitoring Spectrometer
295	GEOS-FP	Goddard Earth Observing System–Forward Processing
	GFED4	Fourth-generation Global Fire Emissions Database
	GMAO	Global Modeling and Assimilation Office
	GOME(-2)	Global Ozone Monitoring Experiment(-2)
	HCHO	Formaldehyde
300	ISAF	In Situ Airborne Formaldehyde
	KORUS-AQ	Korea-United States Air Quality
	LEO	Low Earth Orbit
	MEGAN	Model of Emissions of Gases and Aerosols from Nature
	NEI	National Emissions Inventory
305	NMVOCs	Non-Methane VOCs
	NOMADSS	Nitrogen, Oxidants, Mercury, and Aerosol Distributions, Sources, and Sinks
	OMI	Ozone Monitoring Instrument
	OMPS	Ozone Mapping and Profiler Suite
	PTR-ToF-MS	Proton-Transfer-Reaction Time-of-Flight Mass Spectrometer
310	RMA	Reduced major axis
	SAO	(Harvard) Smithsonian Astrophysical Observatory
	SCD	Slant Column Density
	SCIAMACHY	Scanning Imaging Absorption spectroMeter for Atmospheric Chartography
	SEAC^{4}RS	Studies of Emissions, Atmospheric Composition, Clouds and Climate Coupling by Regional Surveys
315	SENEX	Southeast Nexus
	SONGNEX	Shale Oil and Natural Gas Nexus
	TEMPO	Tropospheric Emissions: Monitoring of Pollution
	TOGA	Trace Organic Gas Analyzer
	TROPOMI	TROPOspheric Monitoring Instrument
320	VCD	Vertical Column Density

VOCs	Volatile Organic Compounds
WE-CAN	Western wildfire Experiment for Cloud chemistry, Aerosol absorption and Nitrogen
WINTER	The Wintertime INvestigation of Transport, Emissions, and Reactivity

Appendix B

325 *Validation platform*

1. Source code

The validation platform (R scripts) is available at: https://doi.org/10.7910/DVN/KG3XNC.

Please download all the files, and follow the instructions in NOTE to install required R packages and run the script.

Sample scripts for processing aircraft, CTM, and satellite data are available at: https://www.acmrsg.org/datasets.

330 Please use process.R and compute.R for step 2-5.

2. Ingesting additional field campaign data

To process additional field campaign data, a user needs to sample the CTM along the flight tracks. This can be done with GEOS-Chem flight diagnostic (http://wiki.seas.harvard.edu/geos-chem/index.php/Planeflight_diagnostic). Please follow process.R (line 117-381) for processing GEOS-Chem flight diagnostic output files. For other CTMs, similar functionality

335 may need to be developed/used.

3. Preparing CTM data

A user also needs to prepare CTM according to satellite schedules. Please follow process.R (line 384-593) for more.

4. Processing new HCHO retrievals

To validate new HCHO retrievals, a user needs to read, clean, filter, and regrid level 2 satellite data. Please follow process.R

340 (line 595-884) for more.

5. Validation of new HCHO retrievals

Finally, we have a sample script (compute.R) for computing and plotting the validation results.

Acknowledgements

References

Apel, E. C., Hills, A. J., Lueb, R., Zindel, S., Eisele, S., and Riemer, D. D.: A Fast-GC/MS system to measure C_2 to C_4 carbonyls, and methanol aboard aircraft, J. Geophys. Res., 108, 8794, doi:10.1029/2002JD003199, 2003.

Apel, E. C., Emmons, L. K., Karl, T., Flocke, F., Hills, A. J., Madronich, S., Lee-Taylor, J., Fried, A., Weibring, P., Walega, J., Richter, D., Tie, X., Mauldin, L., Campos, T., Weinheimer, A., Knapp, D., Sive, B., Kleinman, L., Springston, S., Zaveri, R., Ortega, J., Voss, P., Blake, D., Baker, A., Warneke, C., Welsh-Bon, D., de Gouw, J., Zheng, J., Zhang, R., Rudolph, J., Junkermann, W., and Riemer, D. D.: Chemical evolution of volatile organic compounds in the outflow of the Mexico City Metropolitan area, Atmos. Chem. Phys., 10, 2353–2375, https://doi.org/10.5194/acp-10-2353-2010, 2010.

Apel, E. C., Hornbrook, R. S., Hills, A. J., Blake, N. J., Barth, M. C., Weinheimer, A., Cantrell, C., Rutledge, S. A., Basarab, B., Crawford, J., Diskin, G., Homeyer, C. R., Campos, T., Flocke, F., Fried, A., Blake, D. R., Brune, W., Pollack, I., Peischl, J., Ryer- son, T., Wennberg, P. O., Crounse, J. D., Wisthaler, A., Mikoviny, T., Huey, G., Heikes, B., O'Sullivan, D., and Riemer, D. D.: Upper tropospheric ozone production from lightning NO_x-impacted convection: Smoke ingestion case study from the DC3 campaign,J. Geophys. Res.-Atmos., 120, 2505–2523, 2015.

Barkley, M. P., De Smedt, I., Van Roozendael, M., Kurosu, T. P., Chance, K., Arneth, A., Hagberg, D., Guenther, A., Paulot, F., Marais, E., and Mao, J.: Top-down isoprene emissions over tropical South America inferred from SCIAMACHY and OMI formaldehyde columns, J. Geophys. Res. Atmos., 118, 6849–6868, 2013.

Barth, M. C., Cantrell, C. A., Brune, W. H., Rutledge, S. A., Crawford, J. H., Huntrieser, H., Carey, L. D., MacGorman, D., Weisman, M., Pickering, K. E., Bruning, E., Anderson, B., Apel, E., Biggerstaff, M., Campos, T., Campuzano-Jost, P., Cohen, R., Crounse, J., Day, D. A., Diskin, G., Flocke, F., Fried, A., Garland, C., Heikes, B., Honomichl, S., Hornbrook, R., Huey, L. G., Jimenez, J. L., Lang, T., Lichtenstern, M., Mikoviny, T., Nault, B., O'Sullivan, D., Pan, L. L., Peischl, J., Pollack, I., Richter, D., Riemer, D., Ryerson, T., Schlager, H., St Clair, J., Walega, J., Weibring, P., Weinheimer, A., Wennberg, P., Wisthaler, A., Wooldridge, P. J., and Ziegler, C.: The Deep Convective Clouds and Chemistry (DC3) Field Campaign, B. Am. Meteorol. Soc., 96, 1281–1309, https://doi.org/10.1175/Bams-D-13-00290.1, 2015.

Cao, H., Fu, T.-M., Zhang, L., Henze, D. K., Miller, C. C., Lerot, C., Abad, G. G., De Smedt, I., Zhang, Q., van Roozendael, M., Hendrick, F., Chance, K., Li, J., Zheng, J., and Zhao, Y.: Adjoint inversion of Chinese non-methane volatile organic compound emissions using space-based observations of formaldehyde and glyoxal, Atmos. Chem. Phys., 18, 15017–15046, https://doi.org/10.5194/acp-18-15017-2018, 2018.

Cazorla, M., Wolfe, G. M., Bailey, S. A., Swanson, A. K., Arkinson, H. L., and Hanisco, T. F.: A new airborne laser-induced fluorescence instrument for in situ detection of formaldehyde throughout the troposphere and lower stratosphere, Atmos. Meas. Tech., 8, 541–552, doi:10.5194/amt-8-541-2015, 2015.

Chan Miller, C., Jacob, D. J., Marais, E. A., Yu, K., Travis, K. R., Kim, P. S., Fisher, J. A., Zhu, L., Wolfe, G. M., Hanisco, T. F., Keutsch, F. N., Kaiser, J., Min, K.-E., Brown, S. S., Washenfelder, R. A., González Abad, G., and Chance, K.: Glyoxal yield from isoprene oxidation and relation to formaldehyde: chemical mechanism, constraints from SENEX aircraft observations, and interpretation of OMI satellite data, Atmos. Chem. Phys., 17, 8725–8738, https://doi.org/10.5194/acp-17-8725-2017, 2017.

Chance, K., Palmer, P. I., Spurr, R. J. D., Martin, R. V., Kurosu, T. P., and Jacob, D. J.: Satellite observations of formaldehyde over North America from GOME, Geophys. Res. Lett., 27, 3461–3464, 2000.

395   Chance, K., and Kurucz, R. L.: An improved high-resolution solar reference spectrum for Earth's atmosphere measurements in the ultraviolet, visible, and near infrared, J. Quant. Spectrosc. Radiat. Transf., 111 (9), 1289–1295, 10.1016/j.jqsrt.2010.01.036, 2010.

Courrèges-Lacoste, G. B., Sallusti, M., Bulsa, G., Bagnasco, G., Veihelmann, B., Riedl, S., Smith, D. J., and Maurer, R.: The Copernicus Sentinel 4 mission: a geostationary imaging UVN spectrometer for air quality monitoring, Proceedings
400   Volume 10423, Sensors, Systems, and Next-Generation Satellites XXI; 1042307, https://doi.org/10.1117/12.2282158, 2017.

Crawford, J. H., and Pickering, K. E.: DISCOVER-AQ Advancing Strategies for Air Quality Observations in the Next Decade, Environ. Manage, 4–7, 2014.

De Smedt, I., Müller, J.-F., Stavrakou, T., van der A, R., Eskes, H., and Van Roozendael, M.: Twelve years of global
405   observations of formaldehyde in the troposphere using GOME and SCIAMACHY sensors, Atmos. Chem. Phys., 8, 4947–4963, doi:10.5194/acp-8-4947-2008, 2008.

De Smedt, I., Van Roozendael, M., Stavrakou, T., Müller, J.-F., Lerot, C., Theys, N., Valks, P., Hao, N., and van der A, R.: Improved retrieval of global tropospheric formaldehyde columns from GOME-2/MetOp-A addressing noise reduction and instrumental degradation issues, Atmos. Meas. Tech., 5, 2933–2949, doi:10.5194/amt-5-2933-2012, 2012.

410   De Smedt, I., Stavrakou, T., Hendrick, F., Danckaert, T., Vlemmix, T., Pinardi, G., Theys, N., Lerot, C., Gielen, C., Vigouroux, C., Hermans, C., Fayt, C., Veefkind, P., Müller, J.-F., and Van Roozendael, M.: Diurnal, seasonal and long-term variations of global formaldehyde columns inferred from combined OMI and GOME-2 observations, Atmos. Chem. Phys., 15, 12519–12545, doi:10.5194/acp-15-12519-2015, 2015.

De Smedt, I., Theys, N., Yu, H., Danckaert, T., Lerot, C., Compernolle, S., Van Roozendael, M., Richter, A., Hilboll, A.,
415   Peters, E., Pedergnana, M., Loyola, D., Beirle, S., Wagner, T., Eskes, H., van Geffen, J., Boersma, K. F., and Veefkind, P.: Algorithm theoretical baseline for formaldehyde retrievals from S5P TROPOMI and from the QA4ECV project, Atmos. Meas. Tech., 11, 2395–2426, https://doi.org/10.5194/amt-11-2395-2018, 2018.

DISCOVER-AQ Science Team: DISCOVER-AQ P-3B Aircraft In-situ Trace Gas Measurements. NASA Langley Atmospheric Science Data Center DAAC, DOI: 10.5067/Aircraft/DISCOVER-AQ/Aerosol-TraceGas, 2014.

420   Emmons, L.: Merged Data Files containing all C-130 1 Second Observations. Version 1.0. UCAR/NCAR - Earth Observing Laboratory. https://data.eol.ucar.edu/dataset/373.045 (last access: Jul. 10, 2019), 2016.

EPA: National Emissions Inventory, version 2 Technical Support Document, 2015, https://www.epa.gov/sites/production/files/2015-10/documents/nei2011v2_tsd_14aug2015.pdf (last access: Jul. 9, 2019), 2011.

425   Fried, A., Cantrell, C., Olson, J., Crawford, J. H., Weibring, P., Walega, J., Richter, D., Junkermann, W., Volkamer, R., Sinreich, R., Heikes, B. G., O'Sullivan, D., Blake, D. R., Blake, N., Meinardi, S., Apel, E., Weinheimer, A., Knapp, D., Perring, A., Cohen, R. C., Fuelberg, H., Shetter, R. E., Hall, S. R., Ullmann, K., Brune, W. H., Mao, J., Ren, X., Huey, L. G., Singh, H. B., Hair, J. W., Riemer, D., Diskin, G., and Sachse, G.: Detailed comparisons of airborne formaldehyde measurements with box models during the 2006 INTEX-B and MILAGRO campaigns: potential
430   evidence for significant impacts of unmeasured and multi-generation volatile organic carbon compounds, Atmos. Chem. Phys., 11, 11867–11894, https://doi.org/10.5194/acp-11-11867-2011, 2011.

Giglio, L., Randerson, J. T., and van der Werf, G. R.: Analysis of daily, monthly, and annual burned area using the fourth-geneartion global fire emissions database (GFED4), J. Geophys. Res. Biogeosci., 118, 317–328, doi:10.1002/jgrg.20042, 2013.

435   González Abad, G., Liu, X., Chance, K., Wang, H., Kurosu, T. P., and Suleiman, R.: Updated Smithsonian Astrophysical Observatory Ozone Monitoring Instrument (SAO OMI) formaldehyde retrieval, Atmos. Meas. Tech., 8, 19–32, https://doi.org/10.5194/amt-8-19-2015, 2015.

González Abad, G., Vasilkov, A., Seftor, C., Liu, X., and Chance, K.: Smithsonian Astrophysical Observatory Ozone Mapping and Profiler Suite (SAO OMPS) formaldehyde retrieval, Atmos. Meas. Tech., 9, 2797–2812,
440   doi:10.5194/amt-9-2797-2016, 2016.

Guenther, A. B., Jiang, X., Heald, C. L., Sakulyanontvittaya, T., Duhl, T., Emmons, L. K., and Wang, X.: The Model of Emissions of Gases and Aerosols from Nature version 2.1 (MEGAN2.1): an extended and updated framework for modeling biogenic emissions, Geosci. Model Dev., 5, 1471–1492, doi:10.5194/gmd-5-1471-2012, 2012.

Herman, J., Spinei, E., Fried, A., Kim, J., Kim, J., Kim, W., Cede, A., Abuhassan, N., and Segal-Rozenhaimer, M.: NO_2 and HCHO measurements in Korea from 2012 to 2016 from Pandora spectrometer instruments compared with OMI retrievals and with aircraft measurements during the KORUS-AQ campaign, Atmos. Meas. Tech., 11, 4583–4603, https://doi.org/10.5194/amt-11-4583-2018, 2018.

Hewson, W., Barkley, M. P., González Abad, G., Bösch, H., Kurosu, T., and Spurr, R.: Development and characterisation of a stateof-the-art GOME-2 formaldehyde air-mass factor algorithm, Atmos. Meas. Tech., 8, 4055–4074, doi:10.5194/amt-8-4055-2015, 2015.

Holtslag, A. and Boville, B.: Local versus nonlocal boundary-layer diffusion in a global climate model, J. Clim., 6, 1825–1842, 1993.

Hu, L., and Permar, W.: PTR-ToF-MS Measurements of NMVOCs, HONO, HCN, CH_3CN Data. Version 1.0. UCAR/NCAR - Earth Observing Laboratory. https://doi.org/10.26023/K9F4-2CNH-EQ0W (last access: Nov. 26, 2019), 2019.

Hu, L., Millet, D. B., Baasandorj, M., Griffis, T. J., Turner, P., Helmig, D., Curtis, A. J., and Hueber, J.: Isoprene emissions and impacts over an ecological transition region in the US Upper Midwest inferred from tall tower measurements, J. Geophys. Res.-Atmos., 120, 3553–3571, 2015.

Jaeglé, L., Thornton, J. A., Brown, S. S., Shah, V., Lopez-Hilfiker, F., Lee, B. H., Haskins, J., Fibiger, D. L., McDuffie, E. E., Sparks, T., Ebben, C. J., Wooldridge, P. J., Cohen, R. C., Veres, P. R., Weinheimer, A. J., Montzka, D. D., Dibb, J. E., Schroder, J. C., Jost, P. C., Day, D. A., Jimenez, J. L., Sullivan, A., Guo, H., Weber, R. J., Green, J. R., Fiddler, M. N., Bililign, S., Campos, T. L., Apel E. C., Blake, N. J., Hall, S. R., Ullmann, K., Wolfe, G. M., DiGangi, J. P., Hanisco, T. F., Leen, J. B.: Sources, Chemistry, and Transport of Pollutants over the Eastern United States During the WINTER 2015 Aircraft Campaign, AGU Fall Meeting, 2015.

Jin, X. and Holloway, T.: Spatial and temporal variability of ozone sensitivity over China observed from the Ozone Monitoring Instrument, J. Geophys. Res.-Atmos., 120, 7229–7246, https://doi.org/10.1002/2015JD023250, 2015.

Jin, X., Fiore, A. M., Murray, L. T., Valin, L. C., Lamsal, L. N., Duncan, B., Folkert Boersma, K., De Smedt, I., Abad, G. G., Chance, K., and Tonnesen, G. S.: Evaluating a space-based indicator of surface ozone-NO_x-VOC sensitivity over midlatitude source regions and application to decadal trends, J. Geophys. Res.-Atmos., 122, 439–461, https://doi.org/10.1002/2017JD026720, 2017.

Khokhar, M., Frankenberg, C., Roozendael, M. V., Beirle, S., Kuhl, S., Richter, A., Platt, U., and Wagner, T.: Satellite observations of atmospheric SO_2 from volcanic eruptions during the time-period of 1996–2002, Adv. Space Res., 36, 879–887, doi:10.1016/j.asr.2005.04.114, 2005.

Kim, J., Jeong, U., Ahn, M., Kim, J. H., Park, R. J., Lee, H., Song, C. H., Choi, Y., Lee, K., Yoo, J., Jeong, M., Park, S. K., Lee, K., Song, C., Kim, S., Kim, Y., Kim, S., Kim, M., Go, S., Liu, X., Chance, K., Chan Miller, C., Al-Saadi, J., Veihelmann, B., Bhartia, P. K., Torres, O., González Abad, G., Haffner, D. P., Ko, D. H., Lee, S. H., Woo, J., Chong, H., Park, S. S., Nicks, D., Choi, W. J., Moon, K., Cho, A., Yoon, J., Kim, S., Hong, H., Lee, K., Lee, H., Lee, S., Choi, M., Veefkind, P., Levelt, P., Edwards, D. P., Kang, M., Eo, M., Bak, J., Baek, K., Kwon, H., Yang, J., Park, J., Han, K. M., Kim, B., Shin, H., Choi, H., Lee, E., Chong, J., Cha, Y., Koo, J., Irie, H., Hayashida, S., Kasai, Y., Kanaya, Y., Liu, C., Lin, J., Crawford, J. H., Carmichael, G. R., Newchurch, M. J., Lefer, B. L., Herman, J. R., Swap, R. J., Lau, A. K., Kurosu, T. P., Jaross, G., Ahlers, B., Dobber, M., McElroy, C. and Choi, Y.: New Era of Air Quality Monitoring from Space: Geostationary Environment Monitoring Spectrometer (GEMS). Bull. Amer. Meteor. Soc., https://doi.org/10.1175/BAMS-D-18-0013.1, 2019.

Kleipool, Q. L., Dobber, M. R., de Haan, J. F., and Levelt, P. F.: Earth surface reflectance climatology from 3 years of OMI data, J. Geophys. Res.-Atmos., 113, D18308, doi:10.1029/2008JD010290, 2008.

KORUS-AQ: An International Cooperative Air Quality Field Study in Korea, available at: https://www-air.larc.nasa.gov/missions/korus-aq/ (last access: Oct. 22, 2019), DOI: 10.5067/Suborbital/KORUSAQ/DATA01, 2016.

Kwon, H.-A., Park, R. J., Jeong, J. I., Lee, S., González Abad, G., Kurosu, T. P., Palmer, P. I., and Chance, K.: Sensitivity of formaldehyde (HCHO) column measurements from a geostationary satellite to temporal variation of the air mass factor in East Asia, Atmos. Chem. Phys., 17, 4673–4686, https://doi.org/10.5194/acp-17-4673-2017, 2017.

Kwon, H.-A., Park, R. J., González Abad, G., Chance, K., Kurosu, T. P., Kim, J., De Smedt, I., Van Roozendael, M., Peters, E., and Burrows, J.: Description of a formaldehyde retrieval algorithm for the Geostationary Environment Monitoring Spectrometer (GEMS), Atmos. Meas. Tech., 12, 3551–3571, https://doi.org/10.5194/amt-12-3551-2019, 2019.

Li, C., Joiner, J., Krotkov, N. A., and Dunlap, L.: A newmethod for global retrievals of HCHO total columns from the Suomi National Polar-orbiting Partnership Ozone Mapping and Profiler Suite, Geophys. Res. Lett., 42, 2515–2522, 2015.

Li, M., Zhang, Q., Kurokawa, J.-I., Woo, J.-H., He, K., Lu, Z., Ohara, T., Song, Y., Streets, D. G., Carmichael, G. R., Cheng, Y., Hong, C., Huo, H., Jiang, X., Kang, S., Liu, F., Su, H., and Zheng, B.: MIX: a mosaic Asian anthropogenic emission inventory under the international collaboration framework of the MICS-Asia and HTAP, Atmos. Chem. Phys., 17, 935 963, https://doi.org/10.5194/acp-17-935-2017, 2017.

Liao, J., Hanisco, T. F., Wolfe, G. M., St. Clair, J., Jimenez, J. L., Campuzano-Jost, P., Nault, B. A., Fried, A., Marais, E. A., González Abad, G., Chance, K., Jethva, H. T., Ryerson, T. B., Warneke, C., and Wisthaler, A.: Towards a satellite formaldehyde – in situ hybrid estimate for organic aerosol abundance, Atmos. Chem. Phys., 19, 2765–2785, https://doi.org/10.5194/acp-19-2765-2019, 2019.

Lin, J.-T. and McElroy, M.: Impacts of boundary layer mixing on pollutant vertical profiles in the lower troposphere: Implications to satellite remote sensing, Atmos. Environ., 44, 1726–1739, 2010.

Marais, E. A., Jacob, D. J., Kurosu, T. P., Chance, K., Murphy, J. G., Reeves, C., Mills, G., Casadio, S., Millet, D. B., Barkley, M. P., Paulot, F., and Mao, J.: Isoprene emissions in Africa inferred from OMI observations of formaldehyde columns, Atmos. Chem. Phys., 12, 6219–6235, doi:10.5194/acp-12-6219-2012, 2012.

Martin, R. V., Parrish, D. D., Ryerson, T. B., Nicks Jr., D. K., Chance, K., Kurosu, T. P., Jacob, D. J., Sturges, E. D., Fried, A., and Wert, B. P.: Evaluation of GOME satellite measurements of tropospheric NO_2 and HCHO using regional data from aircraft campaigns in the southeastern United States, J. Geophys. Res.-Atmos., 109, D24307, doi:10.1029/2004JD004869, 2004.

Millet, D. B., Baasandorj, M., Farmer, D. K., Thornton, J. A., Baumann, K., Brophy, P., Chaliyakunnel, S., de Gouw, J. A., Graus, M., Hu, L., Koss, A., Lee, B. H., Lopez- Hilfiker, F. D., Neuman, J. A., Paulot, F., Peischl, J., Pollack, I. B., Ryerson, T. B., Warneke, C., Williams, B. J., and Xu, J.: A large and ubiquitous source of atmospheric formic acid, Atmos. Chem. Phys., 15, 6283–6304, doi:10.5194/acp-15-6283-2015, 2015.

Molod, A., Takacs, L., Suarez, M., Bacmeister, J., Song, I.-S., and Eichmann, A.: The GEOS-5 Atmospheric General Circulation Model: Mean Climate and Development from MERRA to Fortuna, NASA/TM–2012, 104606, 28, 1–124, 2012.

Müller, M., Mikoviny, T., Feil, S., Haidacher, S., Hanel, G., Hartungen, E., Jordan, A., Märk, L., Mutschlechner, P., Schottkowsky, R., Sulzer, P., Crawford, J. H., and Wisthaler, A.: A compact PTR-ToF-MS instrument for airborne measurements of volatile organic compounds at high spatiotemporal resolution, Atmos. Meas. Tech., 7, 3763–3772, https://doi.org/10.5194/amt-7-3763-2014, 2014.

National Oceanic and Atmospheric Administration (NOAA): SONGNEX 2015 CSD Data Archive, Earth System Research Laboratory, Chemical Sciences Division, available at: https://www.esrl.noaa.gov/csd/projects/songnex/ (last access: Oct. 22, 2019), 2017.

Nowlan, C. R., Liu, X., Janz, S. J., Kowalewski, M. G., Chance, K., Follette-Cook, M. B., Fried, A., González Abad, G., Herman, J. R., Judd, L. M., Kwon, H.-A., Loughner, C. P., Pickering, K. E., Richter, D., Spinei, E., Walega, J., Weibring, P., and Weinheimer, A. J.: Nitrogen dioxide and formaldehyde measurements from the GEOstationary Coastal and Air Pollution Events (GEO-CAPE) Airborne Simulator over Houston, Texas, Atmos. Meas. Tech., 11, 5941–5964, https://doi.org/10.5194/amt-11-5941-2018, 2018.

Palmer, P. I., Jacob, D. J., Chance, K., Martin, R. V., Spurr, R. J. D., Kurosu, T. P., Bey, I., Yantosca, R., Fiore, A., and Li, Q.: Air mass factor formulation for spectroscopic measurements from satellites: Application to formaldehyde retrievals from the Global Ozone Monitoring Experiment, J. Geophys. Res.-Atmos., 106, 14539–14550, 2001.

Palmer, P. I., Jacob, D. J., Fiore, A. M., Martin, R. V., Chance, K., and Kurosu, T. P.: Mapping isoprene emissions over North America using formaldehyde column observations from space, J. Geophys. Res.-Atmos., 108, 4180, doi:10.1029/2002JD002153, 2003.

Pfister, G., Flocke, F., Hornbrook, R., Orlando, J., Lee, S., Schroeder, J., and NASA Langley Research Center: Process-Based and Regional Source Impact Analysis for FRAPPÉ and DISCOVER-AQ 2014, available at: https://www.colorado.gov/airquality/tech_doc_repository.aspx?action=open&file=FRAPPE-NCAR_Final_Report_July2017.pdf (last access: Nov. 02, 2019), 2017.

Pollack, I. B., Lindaas, J., Roscioli, J. R., Agnese, M., Permar, W., Hu, L., and Fischer, E. V.: Evaluation of ambient ammonia measurements from a research aircraft using a closed-path QC-TILDAS operated with active continuous passivation, Atmos. Meas. Tech., 12, 3717–3742, https://doi.org/10.5194/amt-12-3717-2019, 2019.

545 Richter, D., Weibring, P., Walega, J. G., Fried, A., Spuler, S. M., and Taubman, M. S.: Compact highly sensitive multi-species airborne mid-IR spectrometer, Appl. Phys. B, 119, 119–131, 2015.

Scarino, A. J., Obland, M. D., Fast, J. D., Burton, S. P., Ferrare, R. A., Hostetler, C. A., Berg, L. K., Lefer, B., Haman, C., Hair, J. W., Rogers, R. R., Butler, C., Cook, A. L., and Harper, D. B.: Comparison of mixed layer heights from airborne high spectral resolution lidar, ground-based measurements, and the WRF-Chem model during CalNex and
550 CARES, Atmos. Chem. Phys., 14, 5547–5560, doi:10.5194/acp-14-5547-2014, 2014.

Schenkeveld, V. M. E., Jaross, G., Marchenko, S., Haffner, D., Kleipool, Q. L., Rozemeijer, N. C., Veefkind, J. P., and Levelt, P. F.: In-flight performance of the Ozone Monitoring Instrument, Atmos. Meas. Tech., 10, 1957–1986, https://doi.org/10.5194/amt-10-1957-2017, 2017.

Shim, C., Wang, Y., Choi, Y., Palmer, P. I., Abbot, D. S., and Chance, K.: Constraining global isoprene emissions with
555 Global Ozone Monitoring Experiment (GOME) formaldehyde column measurements, J. Geophys. Res.-Atmos., 110, D24301, doi:10.1029/2004JD005629, 2005.

Stavrakou, T., Müller, J.-F., De Smedt, I., Van Roozendael, M., van der Werf, G. R., Giglio, L., and Guenther, A.: Global emissions of non-methane hydrocarbons deduced from SCIAMACHY formaldehyde columns through 2003–2006, Atmos. Chem. Phys., 9, 3663–3679, doi:10.5194/acp-9-3663-2009, 2009.

560 Singh, H. B., Brune, W. H., Crawford, J. H., Flocke, F., and Jacob, D. J.: Chemistry and transport of pollution over the Gulf of Mexico and the Pacific: spring 2006 INTEX-B campaign overview and first results, Atmos. Chem. Phys., 9, 2301–2318, doi:10.5194/acp-9-2301-2009, 2009.

Surl, L., Palmer, P. I., and González Abad, G.: Which processes drive observed variations of HCHO columns over India?, Atmos. Chem. Phys., 18, 4549-4566, https://doi.org/10.5194/acp-18-4549-2018, 2018.

565 Tan, W., Liu, C., Wang, S., Xing, C., Su, W., Zhang, C., Xia, C., Liu, H., Cai, Z., and Liu, J.: Tropospheric NO_2, SO_2, and HCHO over the East China Sea, using ship-based MAX-DOAS observations and comparison with OMI and OMPS satellite data, Atmos. Chem. Phys., 18, 15387–15402, https://doi.org/10.5194/acp-18-15387-2018, 2018.

Toon, O. B., Maring, H., Dibb, J., Ferrare, R., Jacob, D. J., Jensen, E. J., Luo, Z. J., Mace, G. G., Pan, L. L., Pfister, L., Rosenlof, K. H., Redemann, J., Reid, J. S., Singh, H. B., Thompson, A. M., Yokelson, R., Minnis, P., Chen, G., Jucks,
570 K. W., and Pszenny, A.: Planning, implementation, and scientific goals of the Studies of Emissions and Atmospheric Composition, Clouds and Climate Coupling by Regional Surveys (SEAC[4]RS) field mission, J. Geophys. Res.-Atmos., 121, 4967–5009, https://doi.org/10.1002/2015jd024297, 2016.

UCAR/NCAR - Earth Observing Laboratory, Jaegle, L., Shah, V.: 1s Merged dataset of all C-130 observations and GEOS-Chem near-realtime simulations for WINTER. Version 1.1. UCAR/NCAR - Earth Observing Laboratory.
575 https://doi.org/10.5065/D68C9TDX (last access: Jul. 10, 2019), 2016.

Vigouroux, C., Hendrick, F., Stavrakou, T., Dils, B., De Smedt, I., Hermans, C., Merlaud, A., Scolas, F., Senten, C., Vanhaelewyn, G., Fally, S., Carleer, M., Metzger, J.-M., Müller, J.-F., Van Roozendael, M., and De Mazière, M.: Ground-based FTIR and MAX-DOAS observations of formaldehyde at Réunion Island and comparisons with satellite and model data, Atmos. Chem. Phys., 9, 9523–9544, doi:10.5194/acp-9-9523-2009, 2009.

580 Wang, Y., Beirle, S., Lampel, J., Koukouli, M., De Smedt, I., Theys, N., Li, A., Wu, D., Xie, P., Liu, C., Van Roozendael, M., Stavrakou, T., Müller, J.-F., and Wagner, T.: Validation of OMI, GOME-2A and GOME-2B tropospheric NO_2, SO_2 and HCHO products using MAX-DOAS observations from 2011 to 2014 in Wuxi, China: investigation of the effects of priori profiles and aerosols on the satellite products, Atmos. Chem. Phys., 17, 5007–5033, https://doi.org/10.5194/acp-17-5007-2017, 2017.

585 Wang, Y., Wang, Z., Yu, C., Zhu, S., Cheng, L., Zhang, Y., and Chen, L.: Validation of OMI HCHO Products Using MAX-DOAS observations from 2010 to 2016 in Xianghe, Beijing: Investigation of the Effects of Aerosols on Satellite Products, Remote Sens., 11(2), 203, https://doi.org/10.3390/rs11020203, 2019.

Warneke, C., Trainer, M., de Gouw, J. A., Parrish, D. D., Fahey, D. W., Ravishankara, A. R., Middlebrook, A. M., Brock, C. A., Roberts, J. M., Brown, S. S., Neuman, J. A., Lerner, B. M., Lack, D., Law, D., Hübler, G., Pollack, I., Sjostedt, S.,
590 Ryerson, T. B., Gilman, J. B., Liao, J., Holloway, J., Peischl, J., Nowak, J. B., Aikin, K. C., Min, K.-E., Washenfelder, R. A., Graus, M. G., Richardson, M., Markovic, M. Z., Wagner, N. L., Welti, A., Veres, P. R., Edwards, P., Schwarz, J.

16

P., Gordon, T., Dube, W. P., McKeen, S. A., Brioude, J., Ahmadov, R., Bougiatioti, A., Lin, J. J., Nenes, A., Wolfe, G. M., Hanisco, T. F., Lee, B. H., Lopez-Hilfiker, F. D., Thornton, J. A., Keutsch, F. N., Kaiser, J., Mao, J., and Hatch, C. D.: Instrumentation and measurement strategy for the NOAA SENEX aircraft campaign as part of the Southeast Atmosphere Study 2013, Atmos. Meas. Tech., 9, 3063–3093, https://doi.org/10.5194/amt-9-3063-2016, 2016.

Weibring, P., Richter, D., Fried, A., Walega, J., and Dyroff, C.: Ultra-high-precision mid-IR spectrometer II: system description and spectroscopic performance, Appl. Phys. B, 85, 207–218, https://doi.org/10.1007/s00340-006-2300-4, 2006.

Weibring, P., Richter, D., Walega, J. G., and Fried, A.: First demonstration of a high performance difference frequency spectrometer on airborne platforms, Opt. Express, 15, 13476–13495, https://doi.org/10.1364/OE.15.013476, 2007.

Weibring, P., Richter, D., Walega, J. G., Rippe, L., and Fried, A.: Difference frequency generation spectrometer for simultaneous multispecies detection., Opt. Express, 18(26), 27670–27681, doi:10.1364/OE.18.027670, 2010.

Wittrock, F., Richter, A., Oetjen, H., Burrows, J. P., Kanakidou, M., Myriokefalitakis, S., Volkamer, R., Beirle, S., Platt, U., and Wagner, T.: Simultaneous global observations of glyoxal and formaldehyde from space, Geophys. Res. Lett., 33, L16804, doi:10.1029/2006GL026310, 2006.

Wofsy, S. C., Afshar, S., Allen, H. M., Apel, E., Asher, E. C., Bar- letta, B., Bent, J., Bian, H., Biggs, B. C., Blake, D. R., Blake, N., Bourgeois, I., Brock, C. A., Brune, W. H., Budney, J. W., Bui, T. P., Butler, A., Campuzano-Jost, P., Chang, C. S., Chin, M., Commane, R., Correa, G., Crounse, J. D., Cullis, P. D., Daube, B. C., Day, D. A., Dean-Day, J. M., Dibb, J. E., DiGangi, J. P., Diskin, G. S., Dollner, M., Elkins, J. W., Erdesz, F., Fiore, A. M., Flynn, C. M., Froyd, K., Gesler, D. W., Hall, S. R., Hanisco, T. F., Hannun, R. A., Hills, A. J., Hintsa, E. J., Hoffman, A., Hornbrook, R. S., Huey, L. G., Hughes, S., Jimenez, J. L., Johnson, B. J., Katich, J. M., Keeling, R. F., Kim, M. J., Kupc, A., Lait, L. R., Lamarque, J.-F., Liu, J., McKain, K., Mclaughlin, R. J., Meinardi, S., Miller, D. O., Montzka, S. A., Moore, F. L., Morgan, E. J., Murphy, D. M., Murray, L. T., Nault, B. A., Neuman, J. A., Newman, P. A., Nicely, J. M., Pan, X., Paplawsky, W., Peischl, J., Prather, M. J., Price, D. J., Ray, E., Reeves, J. M., Richardson, M., Rollins, A. W., Rosenlof, K. H., Ryerson, T. B., Scheuer, E., Schill, G. P., Schroder, J. C., Schwarz, J. P., St.Clair, J. M., Steenrod, S. D., Stephens, B. B., Strode, S. A., Sweeney, C., Tanner, D., Teng, A. P., Thames, A. B., Thompson, C. R., Ullmann, K., Veres, P. R., Vieznor, N., Wagner, N. L., Watt, A., Weber, R., Weinzierl, B., Wennberg, P., Williamson, C. J., Wilson, J. C., Wolfe, G. M., Woods, C. T., and Zeng, L. H.: ATom: Merged Atmospheric Chemistry, Trace Gases, and Aerosols. ORNL DAAC, Oak Ridge, Ten- nessee, USA, https://doi.org/10.3334/ornldaac/1581, 2018.

Wolfe, G. M., Nicely, J. M., St. Clair, J. M., Hanisco, T. F., Liao, J., Oman, L. D., Brune, W. B., Miller, D., Thames, A., González Abad, G., Ryerson, T. B., Thompson, C. R., Peischl, J., McKain, K., Sweeney, C., Wennberg, P. O., Kim, M., Crounse, J. D., Hall, S. R., Ullmann, K., Diskin, G., Bui, P., Chang, C., and Dean-Day, J.: Mapping hydroxyl variability throughout the global remote troposphere via synthesis of airborne and satellite formaldehyde observations, PNAS, 116 (23) 11171-11180, https://doi.org/10.1073/pnas.1821661116, 2019.

Zhu, L., Jacob, D. J., Mickley, L. J., Marais, E. A., Cohan, D. S., Yoshida, Y., Duncan, B. N., González Abad, G., and Chance, K. V.: Anthropogenic emissions of highly reactive volatile organic compounds in eastern Texas inferred from oversampling of satellite (OMI) measurements of HCHO columns, Environ. Res. Lett., 9, 114004, doi:10.1088/1748-9326/9/11/114004, 2014.

Zhu, L., Jacob, D. J., Kim, P. S., Fisher, J. A., Yu, K., Travis, K. R., Mickley, L. J., Yantosca, R. M., Sulprizio, M. P., De Smedt, I., González Abad, G., Chance, K., Li, C., Ferrare, R., Fried, A., Hair, J. W., Hanisco, T. F., Richter, D., Jo Scarino, A., Walega, J., Weibring, P., and Wolfe, G. M.: Observing atmospheric formaldehyde (HCHO) from space: validation and intercomparison of six retrievals from four satellites (OMI, GOME2A, GOME2B, OMPS) with SEAC^{4}RS aircraft observations over the southeast US, Atmos. Chem. Phys., 16, 13477–13490, https://doi.org/10.5194/acp-16-13477-2016, 2016.

Zhu, L., Mickley, L. J., Jacob, D. J., Marais, E. A., Sheng, J., Hu, L., González Abad, G., and Chance, K.: Long-term (2005–2014) trends in formaldehyde (HCHO) columns across North America as seen by the OMI satellite instrument: Evidence of changing emissions of volatile organic compounds, Geophys. Res. Lett., 44, 7079–7086, https://doi.org/10.1002/2017GL073859, 2017a.

Zhu, L., Jacob, D. J., Keutsch, F. N., Mickley, L. J., Scheffe, R., Strum, M., Abad, G. G., Chance, K., Yang, K., Rappengluck, B., Millet, D. B., Baasandorj, M., Jaegle, L., and Shah, V.: Formaldehyde (HCHO) As a Hazardous Air

Pollutant: Mapping Surface Air Concentrations from Satellite and Inferring Cancer Risks in the United States, Environ. Sci. Technol., 51, 5650–5657, https://doi.org/10.1021/acs.est.7b01356, 2017b.

Zoogman, P., Liu, X., Suleiman, R. M., Pennington, W. F., Flittner, D. E., Al-Saadi, J. A., Hilton, B. B., Nicks, D. K., Newchurch, M. J., Carr, J. L., Janz, S. J., Andraschko, M. R., Arola, A., Baker, B. D., Canova, B. P., Chan Miller, C., Cohen, R. C., Davis, J. E., Dussault, M. E., Edwards, D. P., Fishman, J., Ghulam, A., González Abad, G., Grutter, M., Herman, J. R., Houck, J., Jacob, D. J., Joiner, J., Kerridge, B. J., Kim, J., Krotkov, N. A., Lamsal, L., Li, C., Lindfors, A., Martin, R. V., McElroy, C. T., McLin- den, C., Natraj, V., Neil, D. O., Nowlan, C. R., OSullivan, E. J., Palmer, P. I., Pierce, R. B., Pippin, M. R., Saiz-Lopez, A., Spurr, R. J. D., Szykman, J. J., Torres, O., Veefkind, J. P., Veihelmann, B., Wang, H., Wang, J., and Chance, K.: Tropospheric emissions: Monitoring of pollution (TEMPO), J. Quant. Spectrosc. Ra., 186, 17–39, doi:10.1016/j.jqsrt.2016.05.008, 2017.
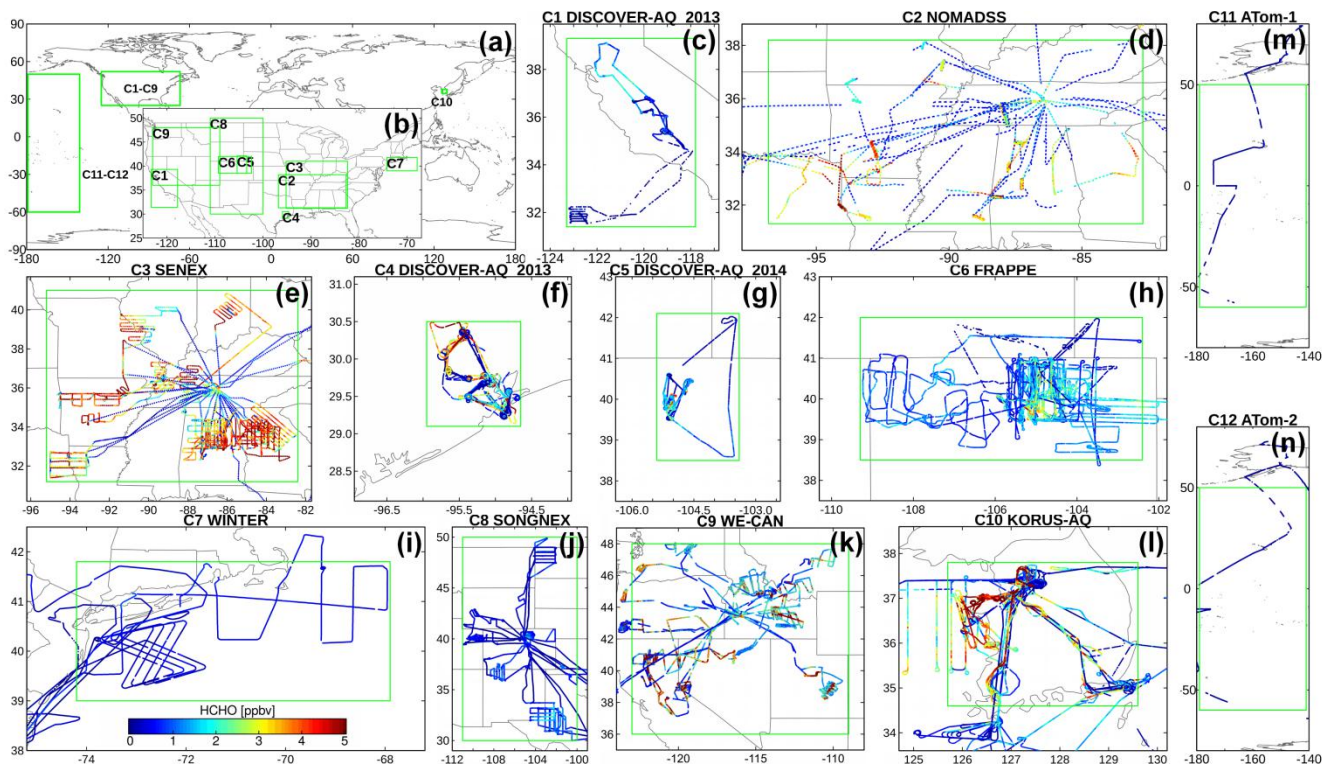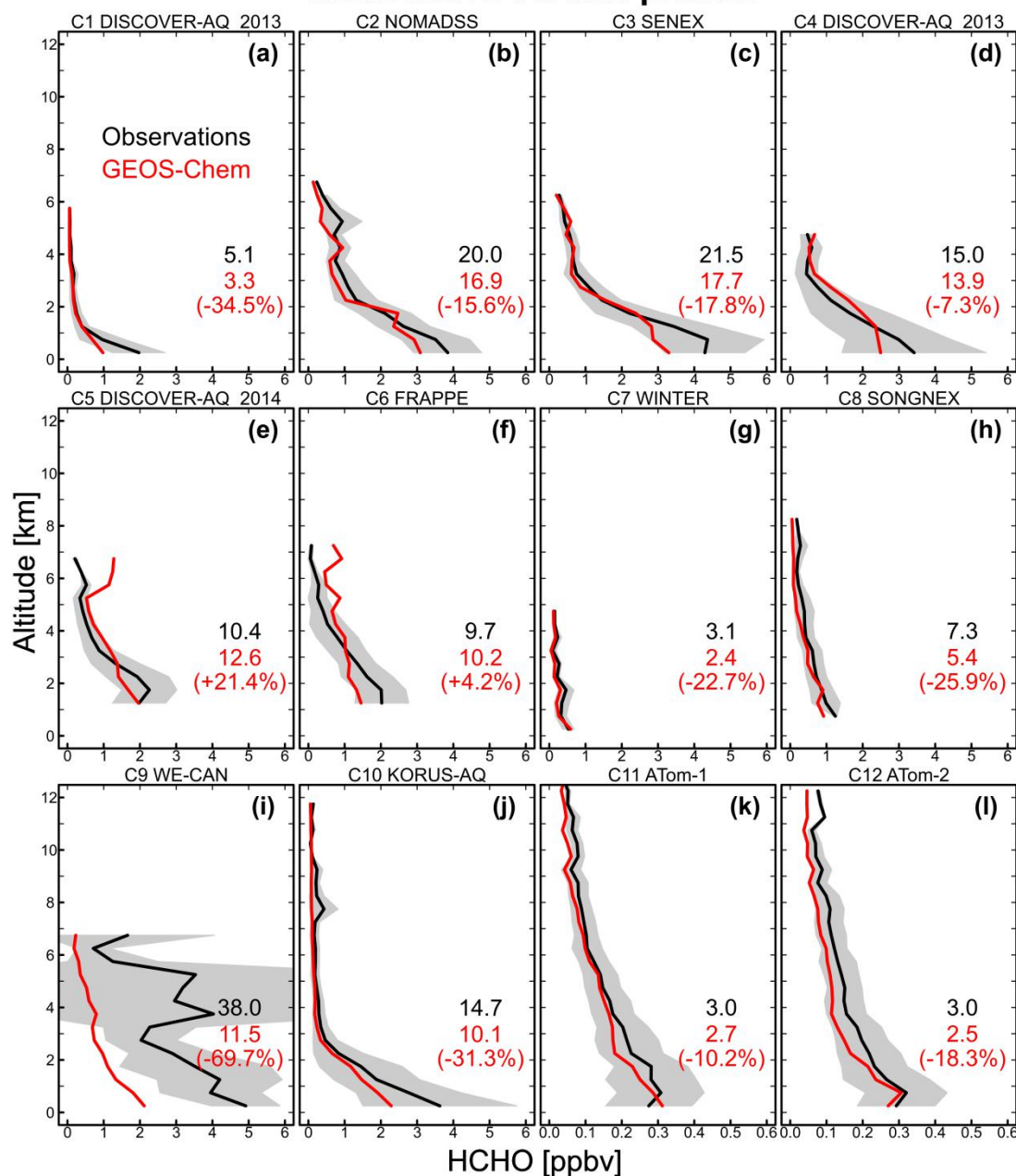
Figure 1. Flight tracks of the 12 aircraft campaigns used in this study. Panel (a) shows the spatial coverage (green rectangles) of the campaigns. Panel (b) (inset) zooms in campaigns over the United States. Aircraft campaigns are numbered as C1–C12. Table 1 summarizes detailed information of the 12 campaigns. Formaldehyde (HCHO) mixing ratios along aircraft flight tracks are shown in panel (c)–(n). Color bar saturates at 5 ppbV. The green rectangle in panel (c)–(n) is the same as that in (a) and (b), indicating spatial domain of a certain campaign. The same domain is also defined in Table 1.

19
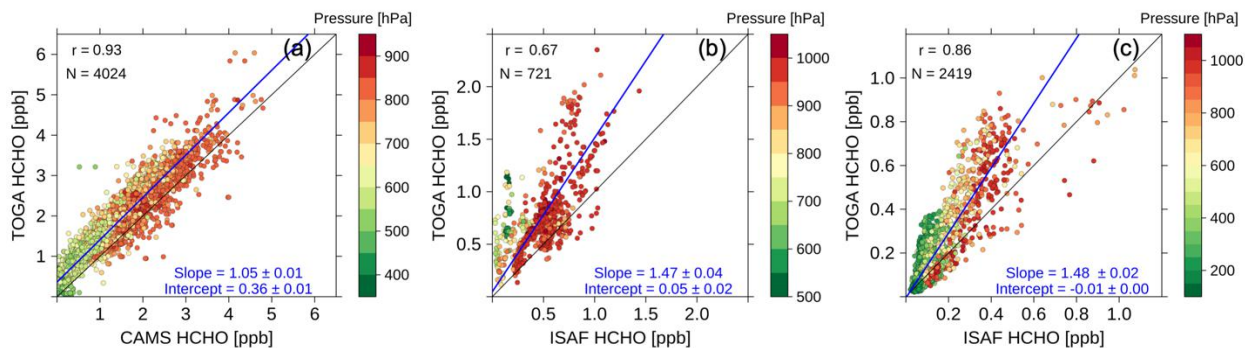
Figure 2. Comparisons between 1-min averaged HCHO observations from multiple instruments. (a) Observations from TOGA and CAMS instruments aboard the NSF/NCAR C-130 during the FRAPPÉ campaign. (b) Observations from TOGA and ISAF instruments aboard the NSF/NCAR C-130 during the WINTER campaign. (c) Observations from TOGA and ISAF instruments aboard the NASA DC-8 during the ATom-2 campaign. HCHO data points are colored by atmospheric pressure. Reduced major axis (RMA) regression slops and intercepts are shown along with the correlation coefficient (*r*), sample size (*N*), RMA regression line (blue) and 1:1 line (black).

Mean HCHO vertical profiles

Figure 3. Mean HCHO vertical profiles as observed during the 12 aircraft campaigns (Table 1) and simulated by GEOS-Chem. GEOS-Chem is sampled along the flight tracks at the time and locations of the measurements. We only use observed and modeled HCHO values within the study area, defined by the green rectangle for each campaign in Figure 1. HCHO values are vertically binned in increments of 500 m. Shading gives the standard deviation in the observations. Observed (black) and modeled (red) HCHO column densities (10^{15} molecules cm^{-2}) are insert along with relative biases (in parentheses) in modeled column densities. The relative biases are further used as correction factors for GOES-Chem columns. Observed column densities are computed using mean observed mixing ratio (black lines), temperature, and pressure. Modeled column densities are computed according to GEOS-Chem HCHO vertical profiles (red lines) as well as temperature and pressure from GEOS-FP. Notice that scale in panel (k) and (l) is different from that in other panels.

21
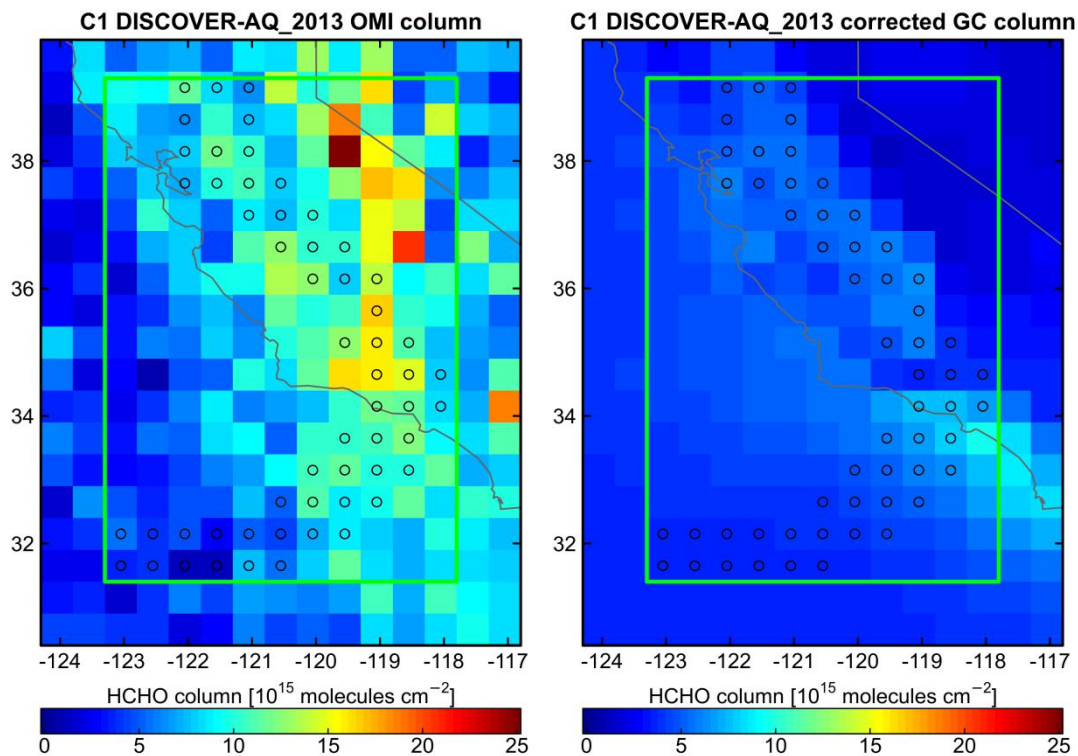
Figure 4. HCHO vertical column densities over California, United States during the DISCOVER-AQ California 2013 (C1; 16 Jan. – 6 Feb.). The left panel shows data from OMI SAO HCHO product. The right panel shows GEOS-Chem model results sampled on the OMI schedule (see text), and scaled by a factor of 1.53 to correct for the bias relative to aircraft measurements (Figure 3). OMI and GEOS-Chem results are regridded onto the 0.5°×0.5° grids. The green rectangles represent the study domain (same as that in Figure 1), which is also defined in Table 1. Here and elsewhere, validation results (*e.g.*, in Table 2) are limited to the grids marked with black open circles, which represent grids that are sampled by the aircraft (*i.e.*, intercepted with flight tracks in Figure 1). .
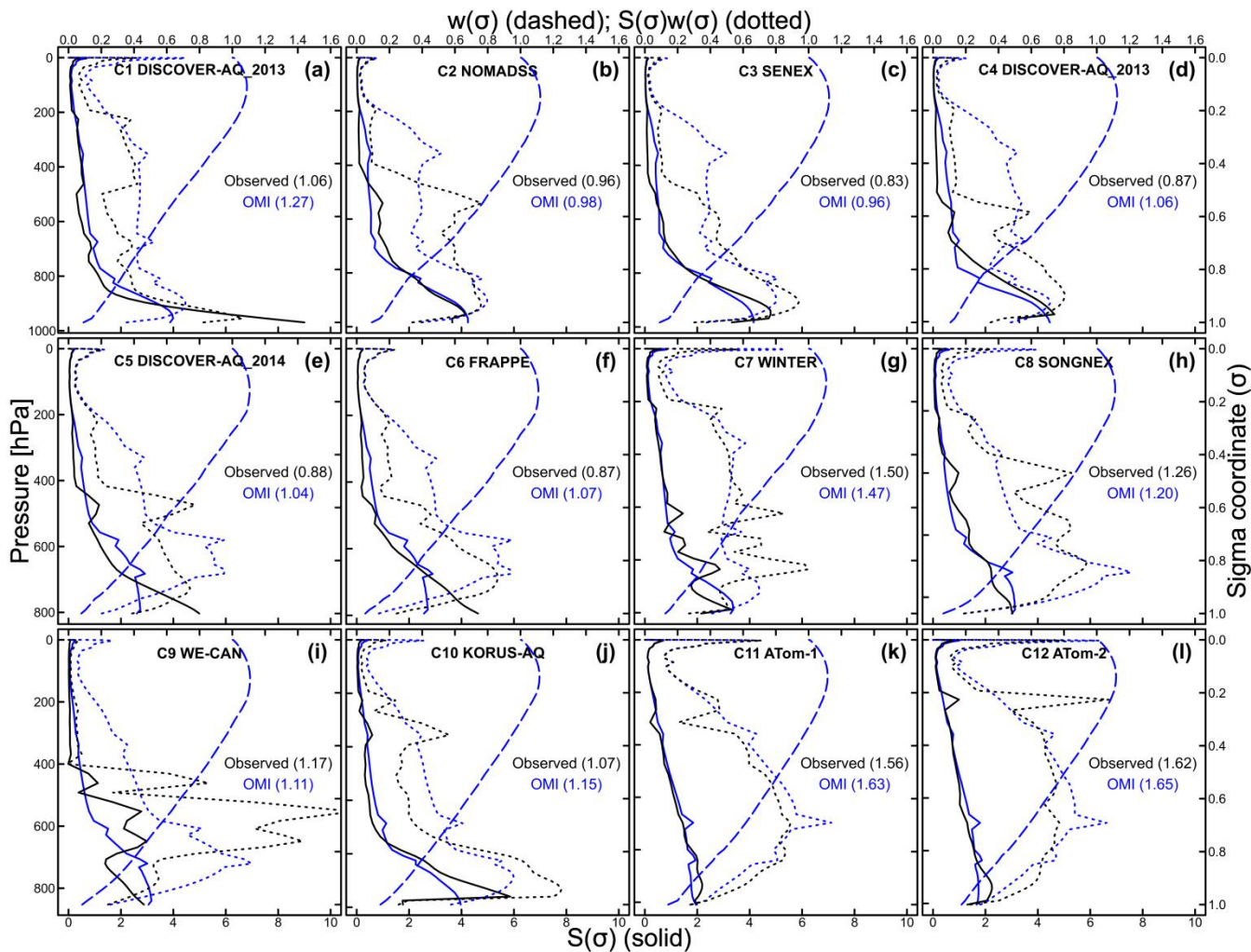
Figure 5. Air mass factor (AMF) components over the 12 aircraft campaigns. Each panel shows mean scattering weights (*w*; blue dashed line) and shape factors (*S*; blue solid line) from OMI SAO HCHO product averaged over the corresponding grids sampled by the aircrafts (marked with open circles in Figure 4 and S1-S11) during the campaign period (defined in Table 1), as well as the product of the two (blue dotted line) from which mean AMF is derived by vertical integration using equation (4). Each panel also shows observed HCHO shape factors (black solid) from the mean HCHO profile in Figure 3. We use mean HCHO profiles from ATom-1 and ATom-2 (Figure 3) to fill observations above 6 km. Also shown is the product (black dotted line) of mean OMI scattering weights (blue dashed line) and observed HCHO shape factor (black solid). Mean AMF values are given in the legend computed using OMI (blue) and observed (black) shape factors.

23

690   **Table 1.** Overview of the 12 aircraft campaigns used in this study

Campaign ID	Campaign name	Region	Date	Platform	HCHO instrument(s) [a]	Domain [b]	References [c]
C1	DISCOVER-AQ California 2013	California, U.S.	Jan. 16–Feb. 06 2013	NASA P-3B	DFGAS (4%)	31.4–39.3N 123.3–117.8W	1, 2
C2	NOMADSS	Southeastern U.S.	Jun. 03–Jul. 14 2013	NSF/NCAR C130	TOGA (15%) [d]	31.3–38.2N 96.8–82.7W	3
C3	SENEX	Southeastern U.S.	Jun. 03–Jul. 10 2013	NOAA WP-3D	ISAF (10%)	31.2–41.0N 95.2–82.4W	4
C4	DISCOVER-AQ Texas 2013	Texas, U.S.	Sep. 04–Sep. 29 2013	NASA P-3B	DFGAS (4%)	29.1–30.5N 95.95–94.65W	1, 2
C5	DISCOVER-AQ Colorado 2014	Colorado, U.S.	Jul. 17–Aug. 10 2014	NASA P-3B	DFGAS (4%)	38.5–42.1N 105.4–103.4W	1, 2
C6	FRAPPÉ	Colorado, U.S.	Jul. 26–Aug. 18 2014	NSF/NCAR C130	CAMS (4%) TOGA (15%) [d]	38.5–42.0N 109.3–102.4W	5, 6
C7	WINTER	Northeastern U.S.	Feb. 03–Mar. 13 2015	NSF/NCAR C-130	ISAF (10%) TOGA (15%) [d]	39.0–41.8N 72.2–67.9W	7
C8	SONGNEX	Western U.S.	Mar. 19–Apr. 27 2015	NOAA WP-3D	ISAF (10%)	30.0–50.0N 111.0–100.0W	8
C9	WE-CAN	Western U.S.	Jul. 26–Sep. 13 2018	NSF/NCAR C-130	PTR-ToF-MS (60%)	36.0–48.0N 123.0–109.0W	9, 10
C10	KORUS-AQ	South Korea	Apr. 26–Jun. 18 2016	NASA DC-8	CAMS (4%)	34.6–37.8N 125.7–129.6W	11
C11	ATom-1	Pacific Ocean	Jul. 29–Aug. 23 2016	NASA DC-8	ISAF (10%)	60.0S–50N 179.0–141.0W	12
C12	ATom-2	Pacific Ocean	Jan. 26–Feb. 21 2017	NASA DC-8	ISAF (10%) TOGA (15%) [d]	60.0S–50N 179.0–141.0W	12

[a] Instrument accuracy is given in parentheses. During C6, C7, and C12, HCHO is measured by two independent instruments
[b] Shown as green rectangles in Figure 1
[c] 1 Crawford and Pickering [2014]; 2 DISCOVER-AQ Science Team [2014]; 3 Emmons [2016]; 4 Warneke et al. [2016]; 5 Pfister et al. [2017]; 6 Richter et al. [2015]; 7 UCAR/NCAR - Earth Observing Laboratory et al. [2016]; 8 National Oceanic and Atmospheric
695   Administration (NOAA) [2017]; 9 Pollack et al. [2019]; 10 Hu and Permar [2019]; 11 KORUS-AQ [2016]; 12 Wofsy et al. [2018]
[d] TOGA has an accuracy of 15% or better

Table 2. HCHO columns and validation results over the 12 aircraft campaigns [a]

Campaign ID	GEOS-Chem columns			OMI						with observed shape factors	
	Original [b]	Corrected [c]	r [d]	AMF_G	AMF	Ω_S [e]	Ω_{S0} [f]	Ω_{avg} [g]	Ω_{comp} [h]	AMF [i]	Ω_{comp} [j]
C1	2.86	4.37	-0.08	3.14	1.21	14.13	4.90	8.90 (+103.9%)	7.63 (+74.7%)	1.06	8.67 (+98.7%)
C2	15.47	18.33	-0.17	2.54	0.97	15.41	4.89	11.59 (−36.8%)	10.85 (−40.8%)	0.96	10.97 (−40.1%)
C3	14.88	18.11	-0.05	2.49	0.93	15.57	4.57	12.66 (−30.1%)	11.86 (−34.5%)	0.83	13.26 (−26.8%)
C4	17.89	19.31	0.72	2.68	0.99	17.20	5.06	12.53 (−35.1%)	12.32 (−36.2%)	0.87	13.91 (−28.0%)
C5	6.52	5.37	-0.22	2.51	1.06	12.88	4.05	9.50 (+76.8%)	8.30 (+54.6%)	0.88	10.08 (+87.6%)
C6 [k]	5.64	5.41	-0.13	2.55	1.03	12.45	4.26	9.31 (+72.0%)	7.95 (+46.9%)	0.87	9.47 (+75.0%)
C7 [l]	2.76	3.57	0.30	3.18	1.53	9.14	1.42	6.55 (+83.7%)	5.03 (+41.1%)	1.50	5.14 (+44.0%)
C8	2.93	3.96	-0.27	2.60	1.18	12.46	3.48	8.39 (+112.1%)	7.59 (+91.9%)	1.26	7.12 (+80.0%)
C9	5.61	18.53	0.06	2.60	1.07	13.79	3.75	10.28 (−44.5%)	9.40 (−49.3%)	1.17	8.57 (−53.7%)
C10	7.86	11.45	0.18	2.59	1.13	14.89	5.33	8.96 (−21.7%)	8.47 (−26.0%)	1.07	8.93 (−22.0%)
C11	2.70	3.01	0.49	2.75	1.56	9.21	1.47	5.20 (+72.9%)	4.95 (+64.5%)	1.56	4.96 (+64.8%)
C12 [l]	2.42	2.95	0.25	2.78	1.71	9.57	1.91	4.91 (+66.1%)	4.50 (+52.1%)	1.62	4.75 (+60.7%)
SEAC^{4}RS [m]	15.23	16.90	0.38	2.66	0.95	-	-	10.60 (−37.0%)	-	-	-

[a] Results are spatially and temporally averaged values for the grids sampled by the aircrafts (marked with open circles in Figure 4 and S1-S11) during the study periods (defined in Table 1). HCHO columns (GEOS-Chem columns, Ω_S, Ω_{S0}, Ω_{avg}, and Ω_{comp}) are in the unit of 10^{15} molecules cm^{-2}. For each aircraft campaign, biases relative to the corrected GEOS-Chem column are given in parentheses
[b] sampled from the GEOS-Chem models according to OMI's schedule
[c] corrected with the factors informed by comparison of observed and modeled HCHO columns (Figure 3)
[d] spatial correlation between GEOS-Chem and OMI HCHO column over the study region (green rectangles in Figure 1)
[e] SCD computed using vertical column density without reference sector correction ("ColumnAmount" data field in OMI SAO HCHO product) and air mass factor (AMF)
[f] SCD correction term recomputed using averaged OMI Ω_S, Ω_{avg}, and AMF following equation (1)

[g] mean VCD by directly averaging valid satellite pixels

[h] VCD recomputed using averaged OMI Ω_S, Ω_{S0}, and AMF following equation (1)

[i] recomputed using averaged OMI AMF_G, observed mean HCHO shape factors (Figure 5), and mean OMI scattering weights (Figure 5) following equation (3)–(5)

[j] VCD computed using recomputed AMF, averaged OMI Ω_S, and averaged OMI Ω_{S0} following equation (1)–(2)

[k] using CAMS observations

[l] using ISAF observations

[m] results reported by Zhu et al. [2016] over the southeastern United States (30.5–39.0N, 95.0–81.5W) during Aug. 05–Sep. 25, 2013. Results are based on a different version of GEOS-Chem model